Materials Research. 2025; 28(suppl. 1): e20250007
DOI: https://doi.org/10.1590/1980-5373-MR-2025-0007

The Effect of Substrate Chemical Homogeneity on Nanotube Formation in Ti-35Nb-xSi Alloys

***Elisiane de Santana Chaves*[a], *Gusttavo Reis Leite Matos*[a]*, *Sandra Andreia Stwart de Araujo Souza*[a], *Edvaldo Alves de Souza*[b], *Michelle Cardinale Souza Silva Macedo*[a]**

[a]*Universidade Federal de Sergipe, Departamento de Ciência e Engenharia de Materiais, 49107-230, São Cristóvão, SE, Brasil.*
[b]*Universidade Federal de Sergipe, Departamento de Física, 49100-000, São Cristóvão, SE, Brasil.*

Received: January 3, 2025; Revised: May 13, 2025; Accepted: June 29, 2025

Modifying the surface of β-Ti alloys using the electrochemical anodizing process makes it possible to produce TiO_2 nanotubes and nanopores that favor better bioactivity and cell-implant interaction. The use of elements that benefit biological properties, such as Nb and Si, makes the whole process even more advantageous. However, the microstructural and compositional characteristics of β-Ti alloys affect the formation, organization and uniformity of nanotubes. Therefore, this study produced Ti-35Nb-xSi alloys and analyzed the microstructure and formation of TiO_2 nanostructures in the as-cast and water quenched (WQ) conditions. The results showed that the addition of Si reduced the precipitation of the ω-phase, making the β-phase more stable and formed the $(Ti,Nb)_5Si_3$ compound for as-cast and $(Ti,Nb)_3Si$ compound for WQ. The growth of nanostructured and hydrophilic layers was benefited from the chemical homogeneity of the substrate after heat treatment, with Si-rich regions affecting nanotube formation and the size of their diameters.

Keywords: *Biomaterials, titanium alloys, Ti-Nb-Si, microstructure, anodization.*

1. Introduction

β-Ti alloys are in considerable demand in the biomaterial area, especially in the orthopaedic and dental sectors, where their purpose is to make prostheses to replace damaged bone structures. Their main advantages are related to their good mechanical strength associated with a low elastic modulus, high resistance to corrosion in body fluids, and appreciable biocompatibility with biological tissues[1-3].

In this respect, some alloying elements that promote the stability of the β-Ti phase are preferred in the manufacture of biocompatible titanium alloys[4,5]. Among these elements, Nb is considered an excellent β-stabilizer and stands out among other competing elements, such as Mo and Ta, because it has a lower melting temperature, making the casting process more economical[6]. In addition, the presence of Nb in Ti-based alloys provides better corrosion resistance due to the formation of Nb_2O_5, as well as contributing to the formation of apatites which are important for the formation of bone tissue[6-10]. Another notable element is Si, whose main promising characteristics are its β-stabilizing effect, low cost, low density and high biocompatibility, as well as being a trace element that stimulates bone mineralization and is essential for cell metabolism[11,12].

The microstructure and properties of Ti-Nb-Si alloys have been investigated in recent years[13-18]. Tavares et al.[15] reported, in particular, the fundamental role of low Si contents in reducing the elastic modulus of the Ti-35Nb alloy, independent of the cooling rate adopted after solubilization heat treatment. The presence of Si in Ti-Nb alloys has also shown benefits in terms of hardness through the mechanisms of solid solution hardening and precipitation of intermetallic compounds[16,17]. Regarding the corrosion resistance, the addition of the elements Nb and Si to Ti led to the formation of Nb_2O_5, SiO_2 and Si doped TiO_2, which increased the barrier properties against the aggressive action of Cl^- ions present in physiological fluids[14].

In parallel with mechanical and corrosive behavior, the interaction between the implant and bone tissue cells is a significant factor to be considered and, in this case, polished metal surfaces or those with flat oxide layers do not promote the ideal interaction that accelerates the process of apatite formation *in vivo* or in simulated body fluid (SBF)[19,20]. Therefore, some methods of surface modification, such as electrochemical anodizing, enable the formation of nanostructured oxides that give a surface with roughness and wettability more suitable for the deposition of hydroxyapatite, adhesion, and proliferation of osteoblastic cells, which means that they increase the rate of osseointegration[21-25]. Another benefit associated with nanostructured oxides is increased corrosion resistance, as they can difficult the infiltration of the corrosive medium into the substrates[26].

Obtaining ordered nanostructures and their geometry, whether nanotubes (NTs) or nanopores (NPs), depends

*e-mail: gusttavoreis@academico.ufs.br
Associate Editor: Igor Vasconcelos.
Editor-in-Chief: Luiz Antonio Pessan.

mostly on the requirements adopted for the process. The literature shows a considerable number of studies on the influence of anodizing parameters (voltage, and time), the electrolyte nature (water, fluoride, and pH concentrations), magnetic stirring, and electrolyte reuse on the synthesis of these structures in commercially pure Ti (CP-Ti)[22,27]. On the other hand, when the material of interest is a titanium alloy, other influential factors must also be considered, such as the type, quantity and distribution of crystalline phases and their chemical compositions. In this regard, some studies have also reported on the role of alloying elements in the stability of the phases and in the different growth mechanisms of TiO_2 [26,28-30].

However, to this moment, no reports have been found in the literature about the characterization of the formation and morphology aspects of TiO_2 oxide synthesized by the electrochemical anodization method in alloys of the Ti-Nb-Si system and, in view of this, this study aimed to investigate the microstructural characteristics and the effect of the chemical homogeneity of the Ti-35Nb-xSi alloy substrate on the formation of TiO_2 nanostructures.

2. Experimental Procedure

2.1. Preparation of Ti-35Nb-xSi alloys

High purity elements were used to prepare the alloys (Ti (94.84%), Nb (99.99%) and Si (99.99%)), whose masses were measured on a semi-analytical balance, with their values corresponding to those of the nominal compositions (Ti-35Nb-xSi with x = 0, 0.5 and 1 wt.%), resulting in a total mass of 100 g for each ingot. Melting was carried out in an arc furnace under an Ar atmosphere, with a tungsten electrode and a water-cooled copper crucible. The ingots were re-melted a total of six times to ensure complete fusion of the high-purity elements. After the melting process, part of the ingots was preserved in as-cast, and the other part was destined for compositional homogenization heat treatment at 1000 °C for 8 h with water cooling. This heat treatment was carried out in a quartz tube furnace under an Ar atmosphere. The samples without heat treatment were designated as-cast, and the heat-treated and water cooled samples as WQ. The chemical compositions of the Ti-35Nb-xSi alloys were analyzed by X-ray fluorescence spectroscopy (XRF - SHIMADZU EDX-7000). This analysis was carried in a vacuum atmosphere with a measurement time of 100 s and a collimator providing a beam spot with a diameter of 10 mm on the surface of the samples of each composition. The values obtained from five measurements were expressed as the mean ± standard deviation.

2.2. Microstructural characterization

The Ti-35Nb, Ti-35Nb-0.5Si and Ti-35Nb-1.0Si alloys (as-cast and WQ) were subjected to metallographic preparation consisting of grinding with SiC sandpaper up to 1500 mesh, polishing with 3 µm diamond paste and 1 µm alumina suspension. Micrographs of all the samples were then taken using an optical microscope (OM - LEICA DM 2500M) after chemical etching with Kroll's solution (91 mL of H_2O, 6 mL of HNO_3, and 3 mL of HF). For the WQ Ti-35Nb-xSi samples (x = 0.5; 1.0), secondary electron images were also obtained on polished-only surfaces using a scanning electron microscope (SEM - JEOL JCM 5700), operated at 10 kV. Si distribution maps were generated from these samples using energy dispersive spectroscopy (SEM/EDS), and spot analyses were carried out to check the Ti, Nb and Si contents in different regions.

The X-ray diffraction (XRD) patterns of the alloys were obtained through a Shimadzu LabX XRD-6000 diffractometer with monochromatic Cu-Kα radiation (λ = 0.15406 nm), operated at 40 kV and 30 mA, at angular range from 30°–90° (2θ). Rietveld refinement was carried out by means of the General Structure Analysis System II (GSAS-II)[31] to determine the volume fractions of the phases in the as-cast and WQ samples. The Inorganic Crystal Structure Database (ICSD) files were used for identifying the phases and refining the XRD patterns.

2.3. Mechanical characterization

The microhardness test was carried out on the Ti-35Nb-xSi alloys (as-cast and WQ) using the Future Tech FM-800 equipment, applying a load of 1000 gf for 10 s. The samples used were submitted to a metallographic procedure of grinding and polishing with a 1 µm alumina suspension. The values obtained were expressed as the mean ± standard deviation after ten indentations.

2.4. Anodizing treatment of Ti-35Nb-xSi alloys

The electrochemical anodizing procedure was performed in an Autolab 302N Potentiostat/Galvanostat using a three-electrode electrochemical cell: counter electrode (platinum rod), reference electrode (Ag/AgCl), and working electrode (Ti-35Nb-xSi - as-cast and WQ). Prior to anodizing, the samples were grinded up to 1500 mesh and cleaned in an ultrasonic bath of deionized water, ethyl alcohol, and acetone for 15 min. The titanium alloys had an average area of 0.5 cm^2 and were anodized by applying a voltage of 10 V for 2 h. The electrolyte used was glycerol/water (50:50) containing 0.54 mol/L of NH_4F, which was maintained under constant stirring at room temperature. The morphology of the oxide formed after the anodizing procedure was observed using field emission scanning electron microscopy (SEM/FEG - JEOL JCM 7500F).

2.5. Wettability and surface energy

The wettability and surface energy of the Ti-35Nb-xSi alloys (x = 0, 0.5 and 1.0 wt.%) was determined by the contact angle test using the sessile drop method. The surfaces of the anodized titanium alloys were cleaned using ethyl alcohol and acetone in an ultrasonic bath and dried in the open air. The analysis was carried out with two fluids (water and formamide) in an experimental device, where approximately 5 µL of each liquid was applied to each surface. The images were taken immediately after placing the drop on the surface and the contact angle was calculated using the open-source ImageJ software. Subsequently, the surface energy was determined using the Kaelble equation (Equation 1) for the two fluids: ultrapure water and formamide.

$$\gamma_{LV}.[1+\cos\theta] = 2\cdot\left(\gamma_S^d\cdot\gamma_{LV}^d\right)^{0.5} + 2\cdot\left(\gamma_S^p\cdot\gamma_{LV}^p\right)^{0.5} \quad (1)$$

where γ_{LV}^{d} = 21.8 mJ.m^{-2} and γ_{LV}^{p} = 51.0 mJ.m^{-2} for water, as well as γ_{LV}^{d} = 39.0 mJ.m^{-2} and γ_{LV}^{p} = 19.0 mJ.m^{-2} for formamide. All tests were carried out with n = 5 and the results are expressed as the mean ± standard deviation. Analysis of Variance (ANOVA) with a significance level of 95% and Tukey's post hoc test ($p < 0.05$) were also applied to all data.

3. Results and Discussion

3.1. Microstructural analysis of the Ti-35Nb-xSi alloys

Table 1 shows the chemical compositions of the Ti-35Nb-xSi alloys (x = 0; 0.5; 1.0 wt.%) measured by XRF, which are similar to the nominal compositions. Figure 1a-c presents the XRD patterns of the Ti-35Nb-xSi alloys in the as-cast condition, refined by the Rietveld method using the GSAS-II program. Some refinement indicators (GOF and R_w) are shown in Figure 1a-c, with the difference between the observed and calculated patterns represented by a solid blue line near the abscissa axis. The variations in the volume fractions of the phases identified as a function of Si concentration are seen in Figure 1d.

Table 1. Nominal and XRF chemical compositions (wt.%) of Ti-35Nb-xSi alloys.

Nominal Composition (wt.%)	XRF Composition (wt.%)		
	Ti	Nb	Si
Ti-35Nb	65.8 ± 0.2	34.2 ± 0.2	-
Ti-35Nb-0.5Si	65.1 ± 0.2	34.4 ± 0.4	0.5 ± 0.1
Ti-35Nb-1.0Si	64.7 ± 0.4	34.1 ± 0.4	1.2 ± 0.1

Regarding to the Ti-35Nb alloy, Figure 1a, it can be seen that the β and ω phases were formed. In Ti-Nb alloys, it is known that their microstructures are highly dependent on the Nb content, which can result in the coexistence of stable phases (α-Ti and β-Ti) and metastable phases (α', α'' and ω) depending on the processing routes adopted. The presence of these phases essentially affects the mechanical properties of Ti-Nb alloys, which requires controlling their volume fractions in order to obtain more optimized conditions[32-35]. In Ti-Nb alloys with Nb contents of 15 wt.% and 35 wt.%, the moduli of the phases that make up the microstructure show the lowest values, being favorable for biomedical applications[36]. However, the 35 wt.% Nb content becomes attractive due to the β-Ti phase being the majority, having the lowest modulus among the phases of Ti alloys, and also because it allows the controlled precipitation of phases through ageing treatment[33,36,37]. In the case of the as-cast Ti-35Nb alloy, it can be seen that the β-phase is predominant, since it has a volume fraction of 0.871, as shown in Figure 1d.

In relation to the ω-phase, its presence in the XRD pattern of the Ti-35Nb alloy is consistent with studies reported in the literature, which show that the 35 wt.% content of Nb is situated within the range of compositions of the Ti-Nb system that favors the precipitation of this phase[15,38]. The appearance of the ω-phase in the microstructure of β-Ti alloys can occur through quenching (ω_{ath}) and aging (ω_{iso}) procedures[39,40]. Considering that the as-cast condition imposes intermediate cooling rates on the ingots between those obtained when cooling in air and in water, it is reasonable to assume that the phase identified is ω_{ath}, which is formed by the collapse of the planes (111) of the β-phase[39].

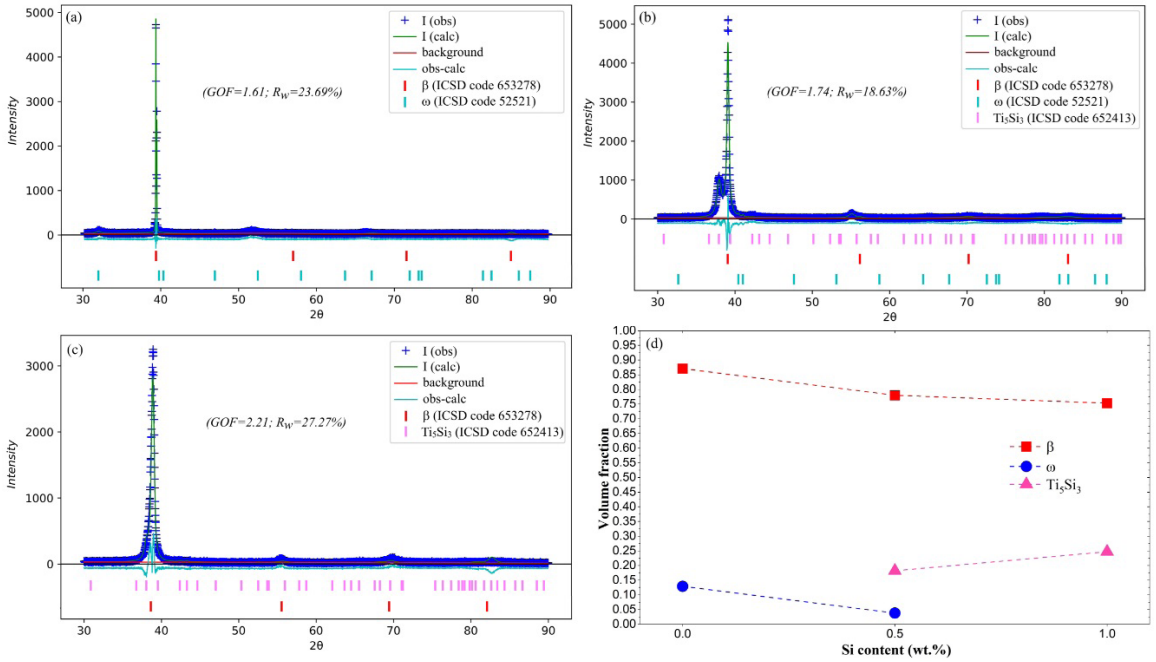

Figure 1. Observed (+) and calculated (solid green line) XRD patterns recorded for the as-cast Ti-35Nb-xSi samples with x = 0 (a), x = 0.5 (b) and x = 1.0 (c). The difference (solid blue line) is shown at the bottom of the image and Bragg reflections are indicated by vertical marks. The ICSD file code for each phase is shown in brackets in the legend. The variation of the volume fractions of the phases recorded as function of Si content in all the as-cast samples are presented in (d).

Figure 1b shows that the ω-phase is still identified in the as-cast Ti-35Nb-0.5Si alloy, but with an estimated volume fraction of 0.038, while in the Si-free alloy this value is 0.129, Figure 1d. Although there are limitations of the XRD technique in detecting phases with low volume fractions in the microstructure and difficulties in refining solid samples, these results, in any case, indicate the existence of a significant reduction of ω-phase due to the presence of Si, which results in greater stability of the β-phase in Ti-Nb-Si alloys[13,15]. In this respect, it is important to note that the ω-phase promotes brittleness, reduces ductility, and increases the elastic modulus in β-Ti alloys, so it is necessary to prevent or control its precipitation in the microstructure[41].

On the other hand, with the additions of 0.5 and 1.0% Si to the Ti-35Nb alloy, peaks referring to the Ti_5Si_3 intermetallic compound (*hP*16 structure)[42] were identified, as shown in Figure 1b, c. The Ti-Si phase diagram shows that this alloying element is an important β-eutectoid stabilizer, which promotes the formation of intermetallic compounds even at low contents, the most stable being Ti_3Si, Ti_5Si_3, Ti_5Si_4, TiSi and $TiSi_2$ in the equilibrium condition. In addition, the maximum solubility of Si in the β-phase is moderately limited, with a content of around 2 wt.% at 1330 °C[43], which is even more restricted in the presence of Nb[15]. Therefore, in as-cast Ti-35Nb-xSi alloys, the increase in Si content should lead to the appearance of a higher volume fraction of Ti_5Si_3, and this is confirmed by the refinements of the XRD patterns, which point to values of 0.182 and 0.247 for 0.5 and 1.0% Si, respectively (Figure 1d).

It is important to note that the Ti-Si and Nb-Si binary systems are analogous and part of their intermetallic compounds are isomorphic, in which the Ti and Nb elements are considered to be soluble[42,44]. In the research by Tian et al.[45] and Guo et al.[46], the authors reported that the Nb_5Si_3 intermetallic compound is a product of direct solidification, given the high cooling rate of the water-cooled copper crucible. Their investigations were carried out on the alloy Nb-22Ti-16Si (at.%) and, due to the solubility of Ti in Nb_5Si_3, this compound is usually referred to as $(Nb,Ti)_5Si_3$. The formation process of $(Nb,Ti)_5Si_3$ in this case was attributed to constitutional undercooling, generated by the rejection of Ti into the liquid phase during the solidification process of the alloy, with the onset of solidification approaching the β(Nb, Ti, Si) + $(Nb,Ti)_5Si_3$ phase field. Similarly, the appearance of $(Ti,Nb)_5Si_3$, or simply Ti_5Si_3, in the Ti-35Nb-0.5Si and Ti-35Nb-1.0Si alloys may also have been due to constitutional undercooling. However, for the compositions in this study, it can be seen that Si is the element rejected at the front of the solid-liquid interface, given its partitioning coefficient, k, of 0.333 relative to Ti[47]. In this way, the rejected Si accumulates, especially in the intergranular region, which favors the formation of intermetallic compounds under casting conditions[15].

The liquidus projection established by Bewlay and Jackson[48] for Ti-Nb-Si alloys located on the Ti-rich side and with low Si contents, the formation of $(Ti,Nb)_5Si_3$ comes from the transition reaction L + $(Nb,Ti)_3Si \rightarrow$ β(Ti, Nb, Si) + $(Ti,Nb)_5Si_3$. In this way, this information certifies the probable solidification path in the Ti-35Nb-xSi alloys (x = 0.5; 1.0), with the peaks of the β and Ti_5Si_3 phases identified through XRD (Figure 1b, c). The microstructures of the as-cast Ti-35Nb-xSi alloys are shown in Figure 2, where

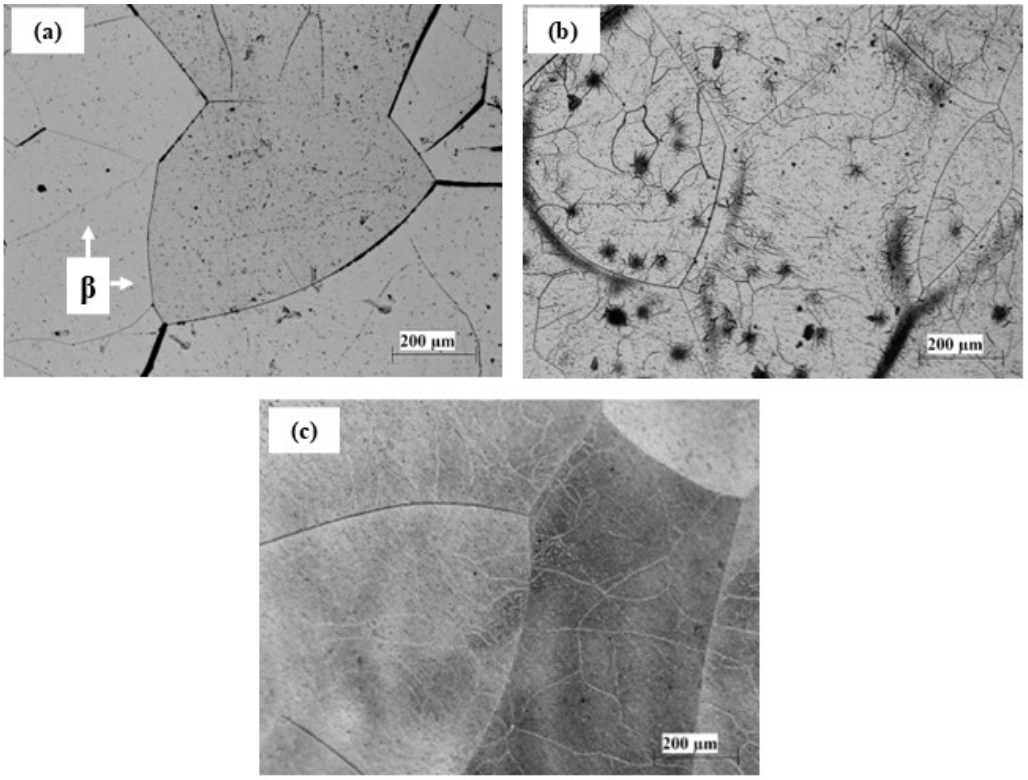

Figure 2. OM images of Ti-35Nb-xSi alloys in the as-cast condition: (a) x = 0, (b) x = 0.5 and (c) x = 1.0.

typical grains of the β-phase can be seen for the Ti-35Nb alloy (Figure 2a). For the Ti-35Nb-0.5Si and Ti-35Nb-1.0Si alloys (Figure 2b, c), it can be seen that their microstructures were more chemically attacked by the Kroll solution, most likely due to the greater reactivity established by the presence of the $(Ti,Nb)_5Si_3$ intermetallic compound. It is important to mention that, to this moment, no studies have been identified in the literature on Ti-35Nb-xSi alloys (x = 0.5; 1.0) in the as-cast condition, most of which focus only on the Ti-Nb-Si system after heat treatment.

Figure 3a-c shows the XRD patterns of the Ti-35Nb-xSi (WQ) alloys, while Figure 3d presents the volume fractions of the phases as a function of Si concentration. Regarding to the Ti-35Nb alloy, only the β and ω phases were identified in the microstructure, with the volume fraction of ω being 0.16 (Figures 3a and 3d). As previously mentioned, rapid cooling conditions, such as water quenching, result in the formation of the ω_{ath}-phase in particular compositions of the Ti-Nb system[15,49-52]. However, Tavares et al.[15] observed the formation of the β, ω_{ath} and α" phases in the Ti-35Nb-0.55Si alloy, differing from the results obtained for the analogous composition in the present study.

It is frequently reported that metastable β-Ti alloys are sensitive to the various processing routes adopted, which can result in diverse microstructures even in similar compositions[49,50]. The α"-phase is also formed through rapid cooling[53], so the literature has reported competitive and/or simultaneous formation between the ω_{ath} and α" phases, from the β-Ti field in alloys of the Ti-Nb system[49,50,52]. According to Moffat and Larbalestier[52], this competition is attributed to the overlapping stabilities of α" and ω_{ath} and their formation temperatures M_s and ω_s, respectively. Slower cooling rates favor the precipitation of ω, while faster rates enable the formation of α". On the other hand, Talbot et al.[49] reported the coexistence of both phases after rapid cooling, where even after the formation of α" when crossing the M_s, there is no impediment to the formation of ω_{ath}. Therefore, it is not trivial to evaluate the competing processes of β-phase decomposition, as several specific factors related to the samples, processing methods and measurement techniques lead to multiple results[50].

The Si present in the Ti-35Nb-0.5Si alloy resulted in the apparent suppression of the ω_{ath}-phase in the WQ condition, given the disappearance of peaks in its XRD pattern (Figure 3b), which is also seen in the Ti-35Nb-1.0Si alloy (Figure 3c). Therefore, the addition of Si in Ti-Nb alloys is beneficial, as this element acts to hinder the collapse of planes (111) of the β-phase and, consequently, the formation of the ω-phase under high cooling rates[13,15]. It should be noted that other alloying elements, e.g. Ta and Zr, can also act as favorable candidates to suppress the formation of the ω_{ath}-phase in Ti-Nb alloys in the WQ condition[51,54]. Abdel-Hady et al.[54] pointed out that Zr is highly effective in suppressing the ω-phase, where Zr contents above 6 mol.% do not enable the identification of peaks corresponding to this phase in the XRD patterns of the Ti-23mol.%Nb alloy (~ 35 wt.% Nb). Souza et al.[51] also found no evidence of the ω_{ath}-phase in the XRD patterns of the Ti-35Nb-xTa alloys (x = 2.5,

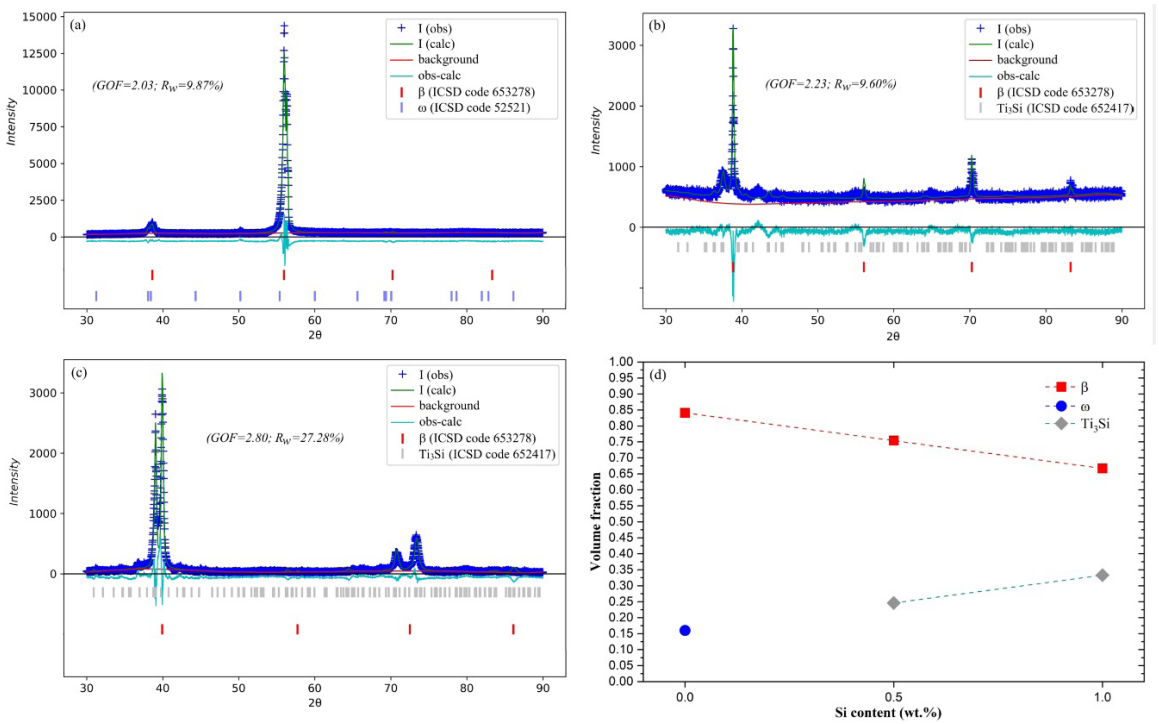

Figure 3. Observed (+) and calculated (solid green line) XRD patterns recorded for the WQ Ti-35Nb-xSi samples with x = 0 (a), x = 0.5 (b) and x = 1.0 (c). The difference (solid blue line) is shown at the bottom of the image and Bragg reflections are indicated by vertical marks. The ICSD file code for each phase is shown in brackets in the legend. The variation of the volume fractions of the phases recorded as function of Si content in all the as-cast samples are presented in (d).

5 and 7.5 wt.%). However, brightfield TEM and selected area diffraction pattern (SADP) analyses confirmed the presence of the ω_{ath}-phase in the microstructures, but with an indication of a reduction in the volume fraction of this phase. In any case, it is important to mention that the positive effect of partial or total ω suppression through Si additions in Ti-35Nb-xSi alloys (as-cast and WQ) occurs at relatively low contents when compared to the Zr and Ta contents adopted in the aforementioned studies, which makes Si an economical alternative for obtaining β-Ti alloys.

On the other hand, the addition of Si resulted in the formation of the Ti_3Si intermetallic compound (*tP*32 structure)[42], which has a different crystal structure and chemical composition to that observed in the as-cast condition. The presence of Ti_3Si in titanium alloys with the additions of Nb and Si, after heat treatment at high temperatures and water quenching, has already been reported in the literature[15,17,55]. Considering the isothermal section at 1000 °C for the Ti-Nb-Si system proposed by Xu et al.[56], whose temperature is the same as the heat treatment in the present study, it is noted that in this condition, the ternary compositions of 0.5 and 1.0% Si, both containing 35% Nb, are in the β-Ti + Ti_3Si two-phase field, as also reported by Tavares et al.[15] for the Ti-35Nb-0.55Si (WQ) alloy. This fact in itself naturally leads to the formation of the Ti_3Si compound, especially when taking into account that these alloys were kept for 8 h at 1000 °C, producing, according to the refinement, Ti_3Si volume fractions of 0.246 and 0.333 for samples containing 0.5 and 1.0% Si, respectively, as seen in Figure 3d. Once again, due to the similarities between the Ti-Si and Nb-Si systems, the intermetallic compounds Ti_3Si and Nb_3Si are isomorphic, but the latter only exists in the temperature range of 1880-1770 °C[48]. In contrast, Nb has high solubility in Ti_3Si and can usually also be referred to as $(Ti,Nb)_3Si$[56].

The microstructures of the Ti-35Nb-xSi (WQ) alloys can be seen in the OM images in Figure 4. Typical β-phase grains are observed in the Ti-35Nb alloy (Figure 4a). The Ti-35Nb-0.5Si and Ti-35Nb-1.0Si alloys (Figure 4b, c) also showed β-phase grains, although once again it can be seen that their microstructures were preferentially attacked by the Kroll solution, which may be related to the presence of the $(Ti,Nb)_3Si$ intermetallic compound. The literature mentions that $(Ti,Nb)_3Si$ appears in the form of very small particles[15,55], which makes it impossible to observe it using OM. Similarly, the ω_{ath}-phase is also not observed in the OM image of the Ti-35Nb alloy (Figure 4a), since this phase appears as nanometric spheroidal or ellipsoidal precipitates dispersed in the β-matrix[57].

Therefore, to investigate the existence of the $(Ti,Nb)_3Si$ intermetallic compound, SEM micrographs and Si distribution maps were obtained on the Ti-35Nb-0.5Si (WQ) and Ti-35Nb-1.0Si (WQ) alloys, as shown in Figure 5. The presence of precipitates is clearly seen in Figure 5a, b, which are preferentially localized on the grain boundaries. The distribution of Si in the microstructures of these alloys (Figure 5c, d) shows its enrichment in these regions, the content of which is 13 wt.%, as shown by the EDS analyses corresponding to point 1 (Table 2). As previously mentioned,

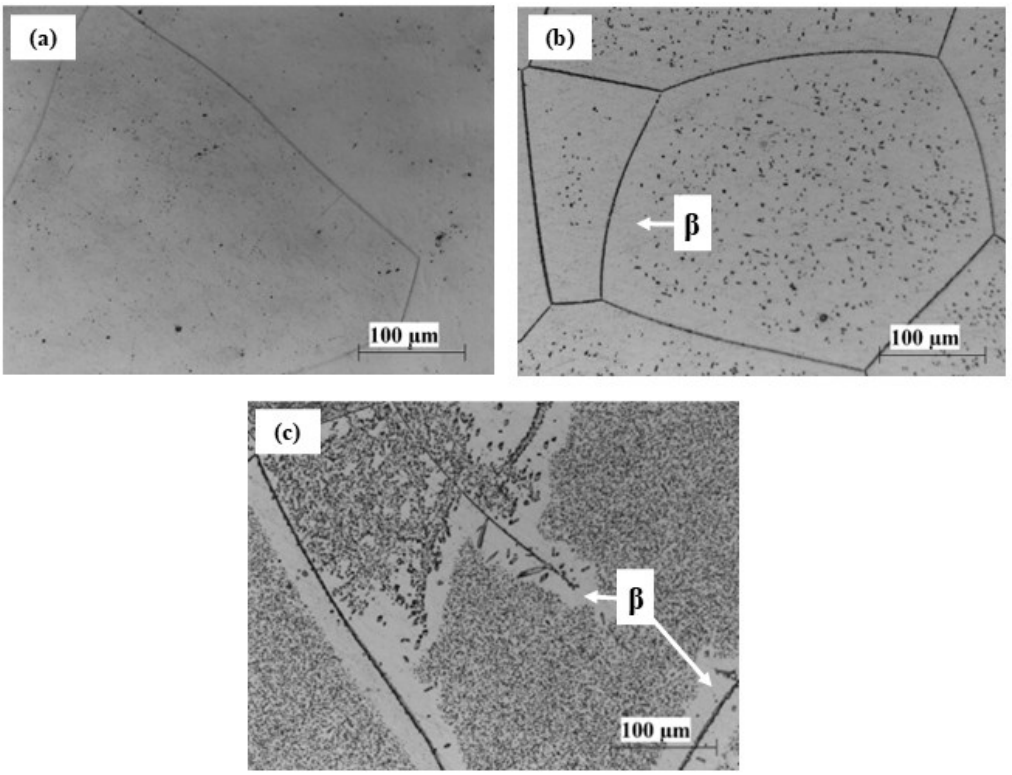

Figure 4. OM images of Ti-35Nb-xSi alloys in the WQ condition: (a) x = 0, (b) x = 0.5 and (c) x = 1.0.

during the solidification process, Si is rejected in front of the solid-liquid interface and is generally confined along the grain boundaries or in interdendritic regions, which are more conducive to the formation of intermetallic compounds[15,58]. It can also be seen that, in the matrix region (point 2, Table 2), the Si content reaches 0.6% for the Ti-35Nb-1.0Si alloy, while in that containing 0.5% Si, its value in the matrix is similar to that of the alloy itself (Table 1). This may indicate that the solubility limit of Si in β-Ti has been reached and/or that there is a decrease in Si in the matrix caused by the formation of a greater volume fraction of $(Ti,Nb)_3Si$ in relation to the alloy with a higher concentration of this element.

3.2. Mechanical analysis of the Ti-35Nb-xSi alloys

The mechanical behavior of the Ti-35Nb-xSi alloys (as-cast and WQ) was evaluated using the Vickers hardness test. Figure 6 shows the variations in hardness values as a function of Si content and processing methods. In the as-cast condition, the values obtained for the Ti-35Nb, Ti-35Nb-0.5Si and Ti-35Nb-1.0Si alloys were 243 ± 5, 215 ± 4 and 247 ± 13 HV, respectively. In the case of the as-cast Ti-35Nb alloy, the result may be due to the contribution of the hardness of the β and especially ω_{ath} phases present in its microstructure, as shown in the XRD patterns in Figure 1a. According to investigations by Lee et al.[36] in the Ti-Nb system, the hardnesses of the phases are presented as: ω > α' > α" > β > α.

The as-cast Ti-35Nb-0.5Si alloy, on the other hand, showed a reduction in hardness, which could, in part, be related to the sharp drop in the density of ω precipitates due to the presence of Si, whose estimated volume fraction is 0.038, while in the Ti-35Nb alloy, the value is 0.129. It is undeniable that Ti_5Si_3 was formed in this alloy with a very significant volume fraction of 0.182 (Figure 1d), and this intermetallic compound denotes an extremely high hardness with a value of around 1154 HV[59]. This could easily compensate for the lower density of ω precipitates and maintain or further increase the hardness, but this is not

Table 2. EDS compositions (wt.%) of WQ Ti-35Nb-xSi alloys (x = 0.5; 1.0).

Nominal Composition (wt.%)	Analyzed Region	EDS Composition (wt.%)		
		Ti	Nb	Si
Ti-35Nb-0.5Si	Point 1 (precipitate)	57.8	29.2	13.0
	Point 2 (matrix)	62.3	37.2	0.5
Ti-35Nb-1.0Si	Point 1 (precipitate)	61.2	25.8	13.0
	Point 2 (matrix)	66.6	32.8	0.6

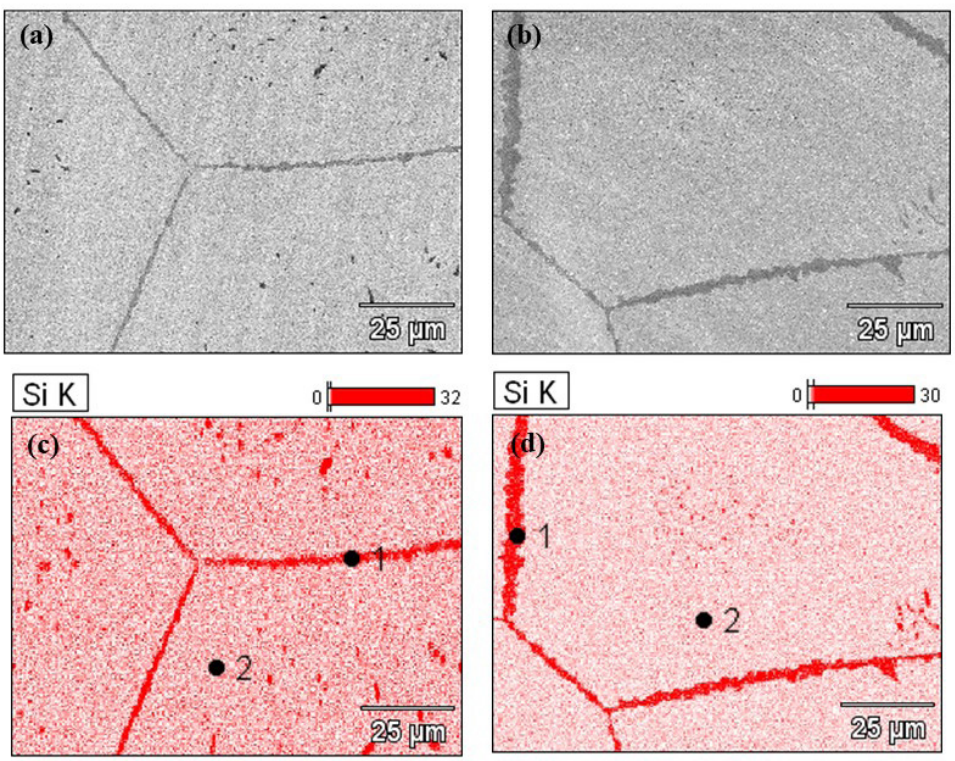

Figure 5. SEM images of Ti-35Nb-xSi alloys in the WQ condition: (a) x = 0.5, (b) x = 1.0 and (c-d) EDS maps of Si distribution, respectively.

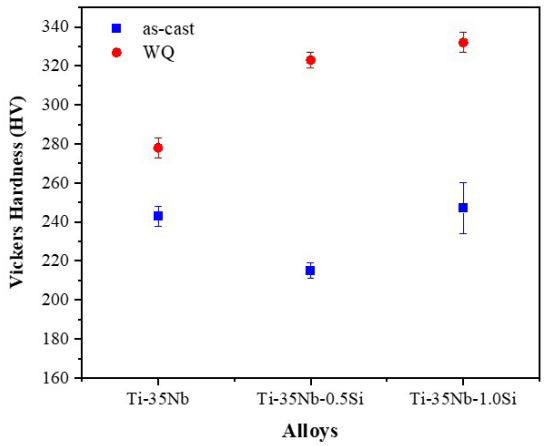

Figure 6. Vickers hardness measurements of Ti-35Nb-xSi alloys in the as-cast and WQ conditions.

the case, which leads to the conclusion that the formation of Ti_5Si_3 particles promotes a strong depletion of Si in the beta the β-matrix, and the influence of the solid solution strengthening is weakened. It is worth noting that, in this alloy, the β-Ti matrix still maintains a high volume fraction of 0.78, and in the literature it is seen that Si in solid solution plays a fundamental role in hardness[60,61] due to the significant difference between the atomic radii of Ti (1.44 Å) and Si (1.18 Å)[62]. For the as-cast Ti-35Nb-1.0Si alloy, the addition of a higher Si-content promotes a more intense saturation of Si into the β-Ti matrix and an increase in hardness, showing a value similar to that obtained for the alloy without Si-content. In this case, it is suggested that the solid solution strengthening effect of Si in the β-Ti matrix is recovered, although there is still a process of Si depletion for the formation of Ti_5Si_3, which is further intensified given the increase in its volume fraction to 0.247.

In the WQ condition, the hardness values for the Ti-35Nb, Ti-35Nb-0.5Si and Ti-35Nb-1.0Si alloys were 278 ± 5, 323 ± 4 and 332 ± 5 HV, respectively. An initial comparison between the processing methods shows that the WQ Ti-35Nb alloy has a higher hardness value when compared to the as-cast condition, which was 243 ± 5 HV. In this respect, it is suggested that the high-temperature compositional homogenization heat treatment contributed to a better elemental distribution and a more effective solid solution strengthening effect. In addition, it should be noted that although in both conditions (as-cast and WQ) there are the same phases: β and ω, the volume fraction of ω that precipitates in the β-Ti matrix in WQ is higher, of 0.16 (Figures 1 and 3), which contributes to a higher hardness value compared to the previous condition.

For the Ti-35Nb-0.5Si and Ti-35Nb-1.0Si alloys in the WQ condition, it can be seen that the additions of Si promote a progressive increase in hardness. In these alloys, the ω-phase is no longer detected (Figure 3b-c) and hardness improvement can also be attributed to solid solution strengthening mechanisms[15], although the presence of the Ti_3Si intermetallic compound also promotes Si depletion from the β-Ti matrix, which is likely to be more intense in the alloy containing 1.0% Si, since it has a higher volume fraction of 0.333 (Figure 3d). A comparison between alloys containing Si in the as-cast and WQ conditions evidently shows that the latter have higher hardnesses, despite Ti_3Si having a lower hardness than Ti_5Si_3. This fact reinforces the understanding that the solid solution strengthening effect is the main mechanism in both groups of alloys, with the type of silicide being responsible for imposing the degree of Si depletion from the β-Ti matrix, i.e., Ti_3Si and Ti_5Si_3 are silicides with different stoichiometries and, in this case, Ti_5Si_3 will require a greater amount of Si for its formation, so this will further weaken the influence of solid solution strengthening on the hardness of as-cast Ti-35Nb-(0.5;1.0) alloys. For WQ alloys containing Si, the better elemental distribution in the matrix due to heat treatment is considered to be a factor that enhances the solid solution strengthening effect.

3.3. Surface morphology of anodized Ti-35Nb-xSi alloys

Figure 7 shows SEM images of the morphology of the oxide film obtained after anodizing the as-cast Ti-35Nb-xSi alloys. It can be seen that the as-cast condition, i.e. not applying the homogenization heat treatment, significantly influenced the anodization behaviour of the Ti-35Nb-xSi alloys under the synthesis parameters of 10 V, 2 h, and 0.54 mol/L of NH_4F in 50:50 water/glycerol. The oxide morphology is almost exclusively lamellar and disordered for all compositions. However, in some areas it was possible to see the formation of nanotubular structures with degenerate aspects, especially in the Ti-35Nb and Ti-35Nb-0.5Si alloys.

However, the literature shows studies on obtaining nanotubes in Ti alloys in the as-cast condition. Ferreira et al.[63] reported that heat treatment at high temperatures and different times was not the key factor in the process of nucleation and growth of NTs, as the same structure was formed in a regular and homogeneous manner in the as-cast Ti-6Al and Ti-6Al-7Nb alloys, under the identical parameters of 20 V, 2 h, and 0.1% vol. of HF. Madian et al.[64] also found the formation of nanotube structures in the as-cast Ti-20Co alloy, using a formamide-based electrolyte containing 0.2 M NH_4F. Additionally, Ding et al.[65] obtained nanotubes in the as-cast Ti-35Nb alloy using an ammonium sulfate electrolyte containing 0.5 wt.% NH_4F. In this study, the authors confirmed that the application of different voltages has a direct response on the formation of NTs and, at low voltages, such as 10 V, only nanoporous layers were formed.

However, it is important to note that the type and contents of the elements present in the substrates can have particular influences on the anodizing process and, in addition, the synthesis parameters (voltage, times, and nature of the electrolyte) may not respond effectively to the chemical nature of each element[66,67]. Thus, it can be seen that the chemical heterogeneity of the Ti-35Nb-xSi alloy substrates (x = 0; 0.5; 1.0 wt.%) may be resulting in elemental segregation that directly impacts on the formation of nanotube structures and, for those small regions where the NTs nucleate and grow disorderedly, there is a compositional balance that benefits the growth of the oxide with this morphological and geometric characteristic.

Figure 8 shows SEM images of the morphology of the oxide film formed after anodizing the WQ Ti-35Nb-xSi alloys. The better distribution of the Ti, Nb and Si elements,

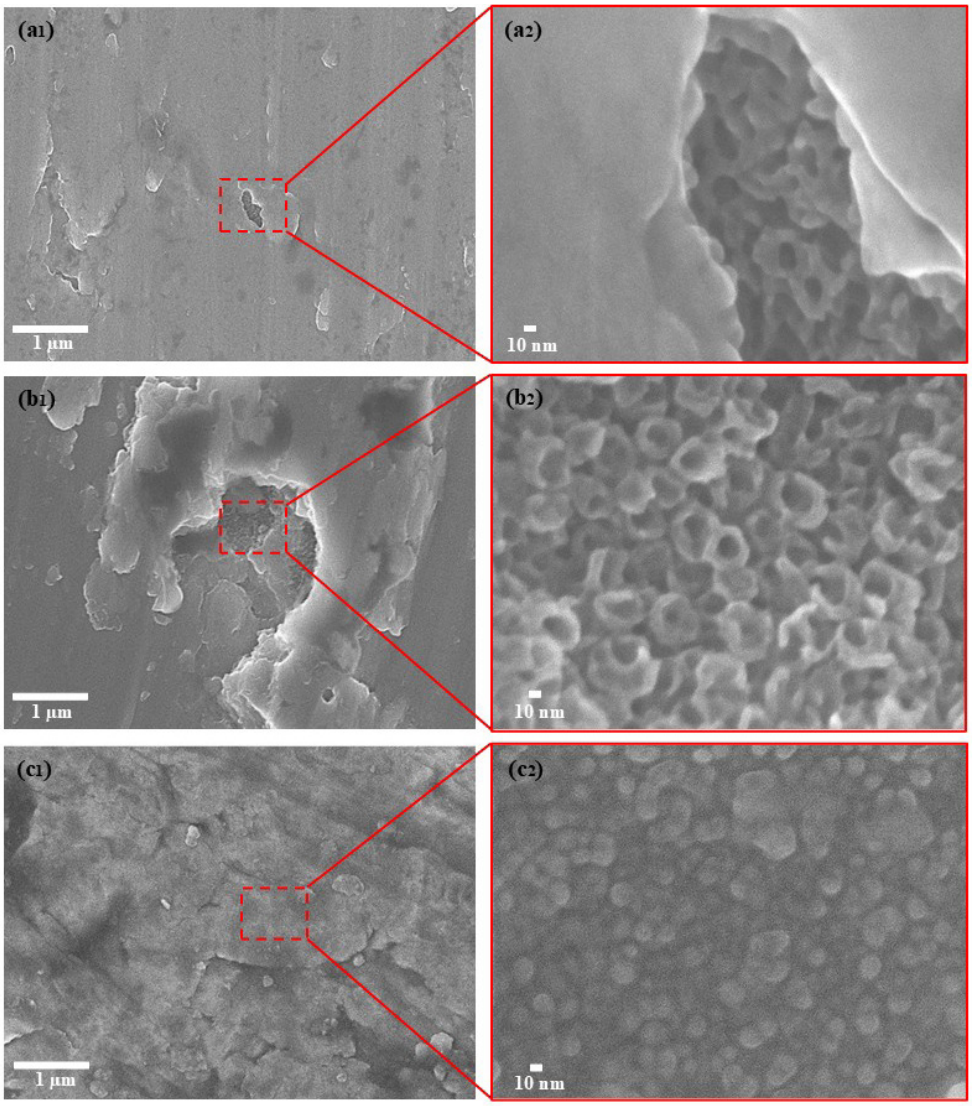

Figure 7. SEM images of as-cast Ti-35Nb-xSi alloys after anodizing for 2 h at 10 V: (a1, a2) x = 0, (b1, b2) x = 0.5 and (c1, c2) x = 1.0.

promoted by diffusion in the heat treatment, evidently resulted in a surface composed of nanotubes and/or nanopores under the same parameters adopted in the synthesis of the alloys in the as-cast condition. In Ti-35Nb alloy (Figure 8a), only the presence of well-defined and uniform TiO_2 nanotubes is observed, similar to those formed in CP-Ti and single-phase Ti alloys[26,29,68,69]. It should be noted that the microstructure of the Ti-35Nb alloy is mostly composed of the β-phase. Luz et al.[28] found that the differences in chemical composition between the α and β phases in the Ti-10Nb alloy provided different morphologies of the nanostructured oxide, with the formation of nanotubes and lamellar structure in the region of predominance of the α and β phase, respectively. Although XRD analysis identified the ω_{ath}-phase in the microstructure of the Ti-35Nb alloy, its chemical composition is similar to the surrounding β-matrix[57] and therefore should not be affecting the growth kinetics of the nanotubes.

The formation of nanotubes in the Ti-35Nb alloy in the WQ condition was also confirmed by Melo et al.[70], however, the internal diameter of the NTs measured in the authors' study was 123 ± 15 nm, compared to the internal diameter of 28.2 ± 0.2 nm in the present study. Here, the answer to the different results can be explained, in particular, by the composition of the electrolytes and the anodizing voltage. Aqueous electrolytes and higher applied voltages, such as the HF solution and 25 V voltage used in the study by Melo et al.[70], increase the diameter of NTs[66].

The Ti-35Nb-0.5Si and Ti-35Nb-1.0Si alloys (Figure 8b, c) also had nanotube layers on the surface of their substrates, but the NTs were smaller and had internal diameters of 23.2 ± 2.7 nm and 18.8 ± 2.1 nm, respectively. In addition to the NTs on the Ti-35Nb-0.5Si and Ti-35Nb-1.0Si alloys, nanoporous layers were also observed (Figure 9), which indicates that the attack of fluoride ions (F^-) has a different action on the

phases present in the microstructures of these alloys. The formation of NPs may be associated with different reaction rates in individual phases[25,30]. It is important to mention that the nanopore corresponds to the initial stage of nanotube formation[28,71]. Thus, the existence of the nanoporous regions in the Ti-35Nb-0.5Si and Ti-35Nb-1.0Si alloys may be related to the greater resistance to the oxidation process of the phase in which the NPs are present.

The microstructure of the WQ Ti-35Nb-0.5Si and Ti-35Nb-1.0Si alloys is composed of the β and $(Ti,Nb)_3Si$ phases, as shown in Figure 4. According to Nascimento et al.[26], the presence of the $(Ti,Nb)_3Si$ intermetallic phase in the Ti-10Mo-xSi alloy delayed the nanopore-nanotube transition by turning the initial TiO_2 layer more resistant to the oxidation and/or dissolution process, which was validated after anodic polarization of the anodized surface, where the nanopore regions remained intact. The study of Tavares et al.[14] found that Si acted as a dopant for TiO_2 and increased the corrosion resistance of Ti-35Nb-xSi alloys. Thus, the NTs in the WQ Ti-35Nb-xSi alloys have grown essentially in the β-phase, while the NPs are present in the regions of the microstructure where the $(Ti,Nb)_3Si$ intermetallic compound is arranged.

The NPs of the Ti-35Nb-0.5Si and Ti-35Nb-1.0Si alloys also showed a reduction in diameter as the Si content increased, with values of 16.0 ± 1.2 nm and 8.4 ± 2.8 nm, respectively. This reduction in nanopore diameters can be explained by the oxide's greater resistance to attack by F^- ions, since Si may be acting as a dopant in the primary TiO_2 formed at the start of the anodizing process. In this way, the greater amount of Si in the Ti-35Nb alloy hinders the nucleation and growth of pites which generate the localized dissolution of TiO_2 and, subsequently, the growth of the diameters and morphology of the nanostructures. Figure 10 shows a histogram where it is possible to better observe the reduction in the internal diameters of the NTs and NPs as a function of the addition of Si to the Ti-35Nb alloy.

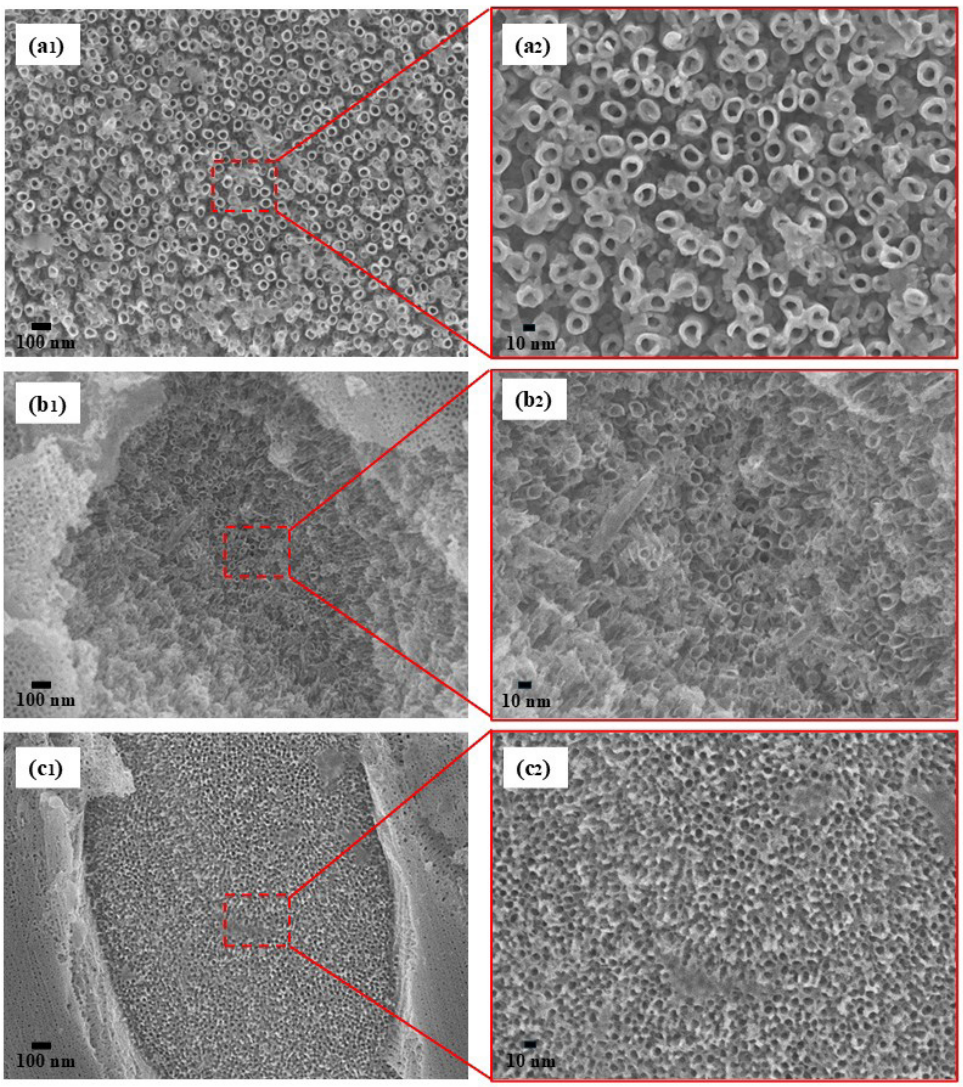

Figure 8. SEM images of WQ Ti-35Nb-xSi alloys after anodizing for 2 h at 10 V showing the presence of nanotubes: (a1, a2) x = 0, (b1, b2) x = 0.5 and (c1, c2) x = 1.0.

Chernozem et al.[72] concluded that TiO_2 NTs with smaller tube diameters were more favorable for cell adhesion and growth on Ti-Nb alloys. Therefore, the anodization of Ti-35Nb-0.5Si and Ti-35Nb-1.0 (WQ) alloys, under the experimental parameters adopted, can enable better osseointegration in orthopaedic and dental implants.

3.4. Wettability and surface energy

Figure 11 shows the wettability of the surfaces of the Ti-35Nb-xSi alloys (as-cast and WQ) which were determined by contact angle (θ) using water. It can be seen that the angles obtained for all the samples showed values below 90°, suggesting that the surfaces examined have a hydrophilic behavior, which is beneficial for metal alloys that are produced for orthopedic and dental applications, since this characteristic provides better interactions with physiological fluids and bone tissue cells[73-75]. According to Figure 11, the as-cast Ti-35Nb-xSi (x = 0, 0.5 and 1.0 wt.%) alloys had the following θ values, respectively: 19.6° ± 0.4°, 19.4° ± 0.4° and 20.7° ± 0.4°. It is reasonable to mention that the surfaces anodized in this processing condition generally showed similar wettability, although

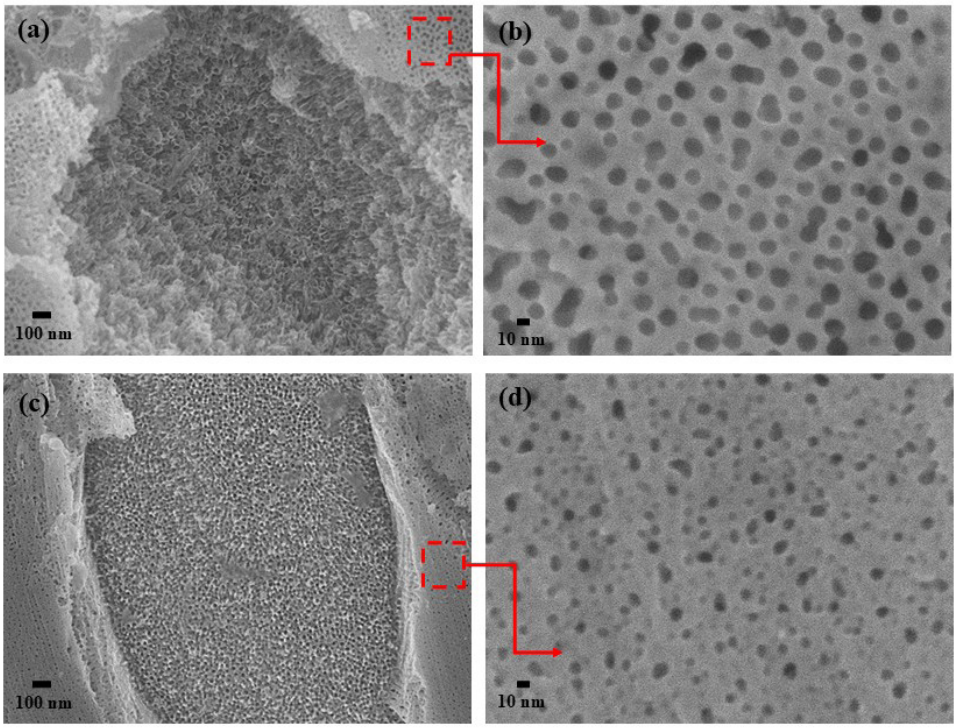

Figure 9. SEM images of WQ Ti-35Nb-xSi alloys after anodizing for 2 h at 10 V showing the presence of nanopores: (a, b) x = 0.5 and (c, d) x = 1.0.

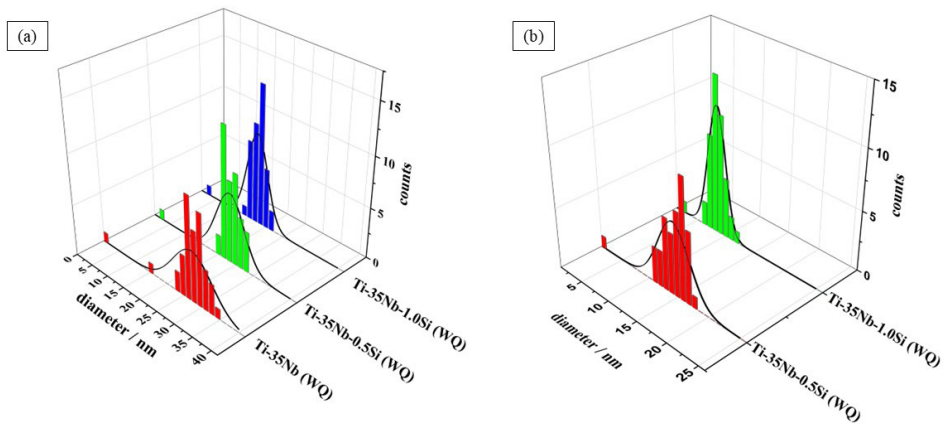

Figure 10. Histogram of the internal diameters of nanotubes (a) and nanopores (b).

there was a subtle statistical difference between the Ti-35Nb and Ti-35Nb-1.0Si alloys. It should be noted that the SEM images of the as-cast Ti-35Nb-xSi alloys showed an oxide with a predominantly lamellar morphology, as well as the presence of small NTs sites with a degenerate appearance (Figure 7).

Regarding to the WQ Ti-35Nb-xSi alloys, the alloy with the addition of 0.5 wt.% Si had a contact angle of 17.1° ± 0.5°, the lowest in this processing condition and also of all the alloys investigated in this study. This result shows that the WQ Ti-35Nb-0.5Si alloy has the most hydrophilic character, i.e. the best wettability, when compared to the angles of 19.7° ± 0.4° and 19.02° ± 0.4° of the Ti-35Nb and Ti-35Nb-1.0Si alloys, respectively. When analyzing the SEM images of the WQ Ti-35Nb-xSi alloys (Figure 8), all the surfaces showed NTs, whose diameters were reduced as the Si content increased. In addition, the alloys with 0.5 wt.% and 1.0 wt.% Si have the presence of NPs which, once again, have their diameters reduced with the gradual increase in Si. This result diverges from the data presented by Liu et al.[73], who stated that hydrophilicity is improved in TiO_2 NTs with larger diameters. On the other hand, it is important to note that the SEM images of the oxide layer in the Ti-35Nb-0.5Si and Ti-35Nb-1.0Si alloys (Figures 8b1 and 8c1) show a more irregular and consequently rougher topography , i.e. marked unevenness, when compared to the Ti-35Nb alloy which showed a more uniform and highly ordered nanotube oxide layer (Figure 8a1).

The topography of nanostructured TiO_2 layers considerably alters the behavior of the water droplet on their surfaces and estimating the level of water penetration into the cavities of nanotubes and nanopores is not trivial[76]. However, Wang et al.[77] found that a nanoporous TiO_2 layer presented a higher contact angle value when compared to a nanotubular TiO_2 layer, in which the result was attributed to the larger spaces existing in a nanotubular structure which allows greater water penetration, since the nanoporous layer denotes a flatter characteristic. As reported in section 3.3, the formation of nanopores in titanium alloys with added Si is associated with the presence of the intermetallic compound Ti_3Si in their microstructures. In this way, it is reasonable to assume that the better wettability for the WQ Ti-35Nb-0.5Si alloy is coherent, as the areas of nanoporous layers, which enable a greater contact angle, can be relatively smaller, since the 0.5 wt.% Si composition showed the lowest volume fraction of Ti_3Si, as indicated in Figure 3d. Moreover, according Liu et al.[73], the increase in roughness and capillary force induced by the disordered nanostructure provides additional force for the penetration or spreading of the liquid. Thus, although the WQ Ti-35Nb alloy has nanotubes with larger internal diameters than the WQ Ti-35Nb-0.5Si alloy, the morphological characteristics of the nanostructured layers of the latter seem to have had a stronger influence on wettability. A comparison between alloys of the same composition and different processing conditions showed that only the Ti-35Nb alloy (as-cast and WQ) showed no statistical difference between the contact angles shown in Figure 11. This result may indicate a similar contact area between the 5 µL water droplet and the lamellar (Figure 7a1) and nanotular (Figure 8a1) oxide layer in the first few moments when it is dripped onto the surface. On the other hand, the WQ Ti-35Nb-0.5Si and Ti-35Nb-1.0Si alloys show a statistical difference in contact angles when compared to the as-cast condition, which may be related to the presence of a more irregular topography and therefore rougher.

Figure 12 shows the surface energy of the Ti-35Nb-xSi alloys (as-cast and WQ) obtained from the Kaelble equation (Equation 1), where the WQ Ti-35Nb-0.5Si alloy had the highest surface energy (70.06 ± 0.19 $mJ.m^{-2}$), showing agreement with the contact angle (θ) made only with water. In general, all the anodized surfaces obtained a surface energy (γ) above 68.7 $mJ.m^{-2}$, which is positive for artificial surfaces that interact with cells[78]. It is important to note that surface energy has an appreciable influence on cellular activities, such as protein adsorption, cell adhesion, growth and proliferation[78] and, in this sense, the Ti-35Nb-xSi alloys (as-cast and WQ) are promising candidates for dental applications, especially the WQ Ti-35Nb-0.5Si and Ti-35Nb-1.0Si alloys, which had the lowest surface energies.

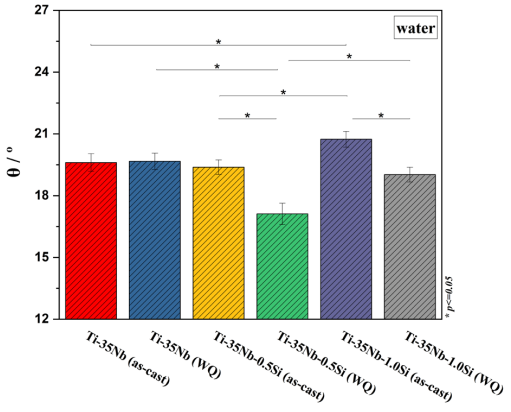

Figure 11. Contact angle values of Ti-35Nb-xSi alloys (as-cast and WQ). Data are expressed as the mean ± standard deviation. (*) Indicates statistical significance between groups (*$p < 0.05$, ANOVA).

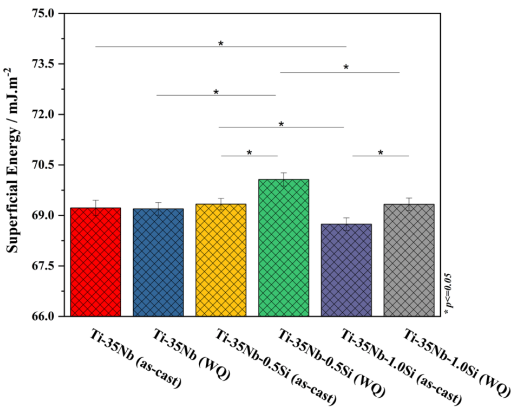

Figure 12. Surface energy values of Ti-35Nb-xSi alloys (as-cast and WQ). Data are expressed as the mean ± standard deviation. (*) Indicates statistical significance between groups (*$p < 0.05$, ANOVA).

4. Conclusions

In this study, the microstructure, mechanical behavior and formation of nanotubes in Ti-35Nb-xSi alloys were analyzed by increasing the Si content and different substrate processing conditions: as-cast and heat treatment at 1000 °C for 8 h followed by water quenching (WQ). Based on the results, Si is a β-stabilizing element that acted to restrict the precipitation of the ω-phase in the as-cast and WQ conditions, since the XRD peaks and volume fractions of this phase were reduced or disappeared. On the other hand, the additions of Si resulted in the formation of the $(Ti,Nb)_5Si_3$ and $(Ti,Nb)_3Si$ intermetallic compounds in the as-cast and WQ conditions, respectively, which contributed to weakening the solid solution strengthening effect which, nevertheless, still remained the main mechanism for increasing hardness, being enhanced by the heat treatment in the WQ condition. The heat treatment applied to the Ti-35Nb-xSi alloy substrates was a key factor in the nucleation and growth of nanotube structures, particularly in the β-phase regions. The results also showed that nanoporous structures were formed in the Ti-35Nb-0.5Si and Ti-35Nb-1.0Si alloys, due to the presence of $(Ti,Nb)_3Si$ which may be increasing the resistance to dissolution of the initial TiO_2 layer formed in the early stages of anodizing. Finally, the nanostructured TiO_2 layers formed on the Ti-35Nb alloys with added Si showed greater resistance to dissolution, since they were more difficult for the nucleation and growth of pites caused by the F^- ions, which resulted in smaller nanopore and nanotube diameters. The Ti-35Nb-xSi alloys (as-cast and WQ) showed hydrophilic characteristics, with the alloys containing Si and in the condition after heat treatment obtaining the best wettability and surface energy results with the WQ Ti-35Nb-0.5Si alloy standing out. It is important to note that the alloys produced for this study are intended for dental applications. Therefore, electrochemical tests are currently being carried out on fluoridated artificial saliva and simulated body fluid (SBF). Bioactivity tests and antibacterial susceptibility tests will also be carried out.

5. Acknowledgments

The authors acknowledge the Brazilian research funding agency CAPES, and UFS for the use of the facilities of the Multiuser Laboratories of Materials Science and Engineering Department (CLMDCEM), the Multiuser Center for Nanotechnology (CMNano), and of the Laboratory of Microstructures and Mechanical Properties (LAMP). We also acknowledge the support of the Physical Metallurgy Laboratory (LABMET/FEM/UNICAMP) for the chemical analysis of the alloys.

6. References

1. Geetha M, Singh AK, Asokamani R, Gogia AK. Ti based biomaterials, the ultimate choice for orthopaedic implants:a review. Prog Mater Sci. 2009;54:397-425.
2. Li Y, Yang C, Zhao H, Qu S, Li X, Li Y. New developments of ti-based alloys for biomedical applications. Materials. 2014;7:1709-800.
3. Elhadad AA, Romero-Resendiz L, Rossi MC, Rodríguez-Albelo LM, Lascano S, Afonso CRM, et al. Findings and perspectives of β-Ti alloys with biomedical applications: exploring beyond biomechanical and biofunctional behaviour. J Mater Res Technol. 2024;33:3550-618.
4. Niinomi M. Mechanical biocompatibilities of titanium alloys for biomedical applications. J Mech Behav Biomed Mater. 2008;1:30-42.
5. Niinomi M, Nakai M, Hieda J. Development of new metallic alloys for biomedical applications. Acta Biomater. 2012;8:3888-903.
6. Zhao D, Han C, Li J, Liu J, Wei Q. In situ fabrication of a titanium-niobium alloy with tailored microstructures, enhanced mechanical properties and biocompatibility by using selective laser melting. Mater Sci Eng C. 2020;111:110784.
7. Jirka I, Vandrovcová M, Frank O, Tolde Z, Plšek J, Luxbacher T, et al. On the role of Nb-related sites of an oxidized β-TiNb alloy surface in its interaction with osteoblast-like MG-63 cells. Mater Sci Eng C. 2013;33(3):1636-45.
8. Bai Y, Deng Y, Zheng Y, Li Y, Zhang R, Lv Y, et al. Characterization, corrosion behavior, cellular response and in vivo bone tissue compatibility of titanium-niobium alloy with low Young's modulus. Mater Sci Eng C. 2016;59:565-76.
9. Wang Q, Han C, Choma T, Wei Q, Yan C, Song B, et al. Effect of Nb content on microstructure, property and in vitro apatite-forming capability of Ti-Nb alloys fabricated via selective laser melting. Mater Des. 2017;126:268-77.
10. Pereira BL, Lepienski CM, Seba V, Hobold G, Soaresd P, Chee BS, et al. Titanium-Niobium (Ti-xNb) alloys with high Nb amounts for applications in biomaterials. Mater Res. 2020;23(6):e20200405.
11. Calin M, Gebert A, Ghinea AC, Gostin PF, Abdi S, Mickel C, et al. Designing biocompatible Ti-based metallic glasses for implant applications. Mater Sci Eng C. 2013;33(2):875-83.
12. Wang Q, Hu H, Qiao Y, Zhang Z, Sun J. Enhanced performance of osteoblasts by silicon incorporated Porous TiO_2 coating. J Mater Sci Technol. 2012;28(2):109-17.
13. Kim HS, Kim WY, Lim SH. Microstructure and elastic modulus of Ti-Nb-Si ternary alloys for biomedical applications. Scr Mater. 2006;54(5):887-91.
14. Tavares AMG, Fernandes BS, Souza SA, Batista WW, Cunha FGC, Landers R, et al. The addition of Si to the Ti-35Nb alloy and its effect on the corrosion resistance, when applied to biomedical materials. J Alloys Compd. 2014;591:91-9.
15. Tavares AMG, Ramos WS, de Blas JCG, Lopes ESN, Caram R, Batista WW, et al. Influence of Si addition on the microstructure and mechanical properties of Ti-35Nb alloy for applications in orthopedic implants. J Mech Behav Biomed Mater. 2015;51:74-87.
16. Tavares AMLG, De Souza EA, Da Silva MSC, Matos GRL, Batista WW, De Araujo Souza SAS. Role of silicon in the microstructural development and properties of Ti-15Nb-xSi alloys for biomedical applications. Mater Res. 2021;24(3):e20200417.
17. Shevchenko OM, Kulak LD, Kuzmenko MM, Firstov SO. Formation of Silicides and their Influence on the structure and properties of cast alloys of the Ti–18Nb–xSi system for biomedical purposes. Mater Sci. 2020;55(4):577-84.
18. Dawood NM, Jassim SA, Khalaf ZH. Effect of Si content on microstructure and mechanical behavior of Porous Ti-22at% Nb shape memory alloys for biomedical applications. Mater Sci Forum. 2023;1089:109-19.
19. Sasikumar Y, Karthega M, Rajendran N. In vitro bioactivity of surface-modified β-Ti alloy for biomedical applications. J Mater Eng Perform. 2011;20(7):1271-7.
20. Kokubo T, Yamaguchi S. Novel bioactive materials developed by simulated body fluid evaluation: surface-modified Ti metal and its alloys. Acta Biomater. 2016;44:16-30.
21. Tsuchiya H, Macak JM, Müller L, Kunze J, Müller F, Greil P, et al. Hydroxyapatite growth on anodic TiO_2 nanotubes. J Biomed Mater Res A. 2006;77(3):534-41.
22. Roy P, Berger S, Schmuki P. TiO_2 nanotubes: synthesis and applications. Angew Chem Int Ed. 2011;50(13):2904-39.

23. Minagar S, Berndt CC, Wang J, Ivanova E, Wen C. A review of the application of anodization for the fabrication of nanotubes on metal implant surfaces. Acta Biomater. 2012;8:2875-88.
24. Oh S, Daraio C, Chen LH, Pisanic TR, Fiñones RR, Jin S. Significantly accelerated osteoblast cell growth on aligned TiO_2 nanotubes. J Biomed Mater Res A. 2006;78(1):97-103.
25. Macak JM, Tsuchiya H, Ghicov A, Yasuda K, Hahn R, Bauer S, et al. TiO_2 nanotubes: self-organized electrochemical formation, properties and applications. Curr Opin Solid State Mater Sci. 2007;11:3-18.
26. Nascimento DS, Matos GRL, Moreira FKV, Macedo MCSS, Souza SA. Anodizing-induced evolution of nanostructural surface morphologies in Ti-10Mo-xSi alloys for enhanced corrosion resistance. Surf Coat Tech. 2019;377:124924.
27. Puga ML, Venturini J, ten Caten CS, Bergmann CP. Influencing parameters in the electrochemical anodization of TiO_2 nanotubes: systematic review and meta-analysis. Ceram Int. 2022;48:19513-26.
28. Luz AR, Santos LS, Lepienski CM, Kuroda PB, Kuromoto NK. Characterization of the morphology, structure and wettability of phase dependent lamellar and nanotube oxides on anodized Ti-10Nb alloy. Appl Surf Sci. 2018;448:30-40.
29. Tang HC, Zhao DP, Wan CJ, Li XS, Ji XW, Tang JC, et al. Influence of heterogeneous microstructures on anodization behavior and biocompatibility of Ti−15Zr alloy. Trans Nonferrous Met Soc China. 2023;33(7):2076-89.
30. Majchrowicz A, Roguska A, Majchrowicz K, Pisarek M, Hołdyński M, Bazarnik P, et al. Influence of microstructural features on the growth of nanotubular oxide layers on β-phase Ti-24Nb-4Zr-8Sn and α + β-phase Ti-13Nb-13Zr alloys. Surf Coat Tech. 2021;425:127695.
31. Toby BH, Von Dreele RB. GSAS-II: the genesis of a modern open-source all purpose crystallography software package. J Appl Cryst. 2013;46(2):544-9.
32. Hon YH, Wang JY, Pan YN. Composition/phase structure and properties of titanium-niobium alloys. Mater Trans. 2003;44(11):2384-90.
33. Thoemmes A, Ivanov IV, Ruktuev AA, Lazurenko DV, Bataev IA. Structure and phase composition of biomedical alloys of the Ti-Nb system in cast condition and after heat treatment. Metal Sci Heat Treat. 2019;60:659-65.
34. Moreno JJG, Bönisch M, Panagiotopoulos NT, Calin M, Papageorgiou DG, Gebert A, et al. Ab-initio and experimental study of phase stability of Ti-Nb alloys. J Alloys Compd. 2017;696:481-9.
35. Fikeni L, Annan KA, Mutombo K, Machaka R. Effect of Nb content on the microstructure and mechanical properties of binary Ti-Nb alloys. Mater Today Proc. 2021;38:913-7.
36. Lee CM, Ju CP, Chern Lin JH. Structure-property relationship of cast Ti-Nb alloys. J Oral Rehabil. 2002;29:314-22.
37. Talbot CEP, Church NL, Jones NG. Effect of prior processing on the decomposition of the β phase in Ti–Nb alloys during intermediate heat treatments. Scr Mater. 2024;238:115729.
38. Illarionov AG, Grib SV, Illarionova SM, Popov AA. Relationship between structure, phase composition, and physicomechanical properties of quenched Ti–Nb alloys. Phys Met Metallogr. 2019;120(2):150-6.
39. Prima F, Vermaut P, Texier G, Ansel D, Gloriant T. Evidence of α-nanophase heterogeneous nucleation from ω particles in a β-metastable Ti-based alloy by high-resolution electron microscopy. Scr Mater. 2006;54(4):645-8.
40. Mello GM, Salvador CF, Cremasco A, Caram R. The effect of Sn addition on phase stability and phase evolution during aging heat treatment in Ti-Mo alloys employed as biomaterials. Mater Charact. 2015;110:5-13.
41. Moraes PEL, Contieri RJ, Lopes ESN, Robin A, Caram R. Effects of Sn addition on the microstructure, mechanical properties and corrosion behavior of Ti-Nb-Sn alloys. Mater Charact. 2014;96:273-81.
42. Zhao JC, Jackson MR, Peluso LA. Mapping of the Nb-Ti-Si phase diagram using diffusion multiples. Mater Sci Eng A. 2004;372(1–2):21-7.
43. Massalski TB, Murray JL, Bennett LH, Baker H. Binary alloy phase diagrams. 2nd ed. Metals Park, OH: American Society for Metals; 1987. (vol. 2)
44. Zhan Y, Sun Z, Jiang J, Ma J, Zhang X, Zhuang Y. The 773 K isothermal section of the ternary phase diagram of the Nb-Ti-Si system. J Alloys Compd. 2009;468(1-2):150-3.
45. Tian YX, Guo JT, Sheng LY, Cheng GM, Zhou LZ, He LL, et al. Microstructures and mechanical properties of cast Nb-Ti-Si-Zr alloys. Intermetallics. 2008;16(6):807-12.
46. Guo E, Singh SS, Kaira CS, Meng X, Xu Y, Luo L, et al. Mechanical properties of microconstituents in Nb-Si-Ti alloy by micropillar compression and nanoindentation. Mater Sci Eng A. 2017;687:99-106.
47. Bermingham MJ, McDonald SD, Dargusch MS, StJohn DH. The mechanism of grain refinement of titanium by silicon. Scr Mater. 2008;58(12):1050-3.
48. Bewlay BP, Jackson MR. The Nb-Ti-Si ternary phase diagram: evaluation of liquid-solid phase equilibria in Nb-and Ti-Rich alloys. J Phase Equilibria. 1997;18(3):264-78.
49. Talbot CEP, Church NL, Hildyard EM, Connor LD, Miller JR, Jones NG. On the stability and formation of the α'' and ω phases in Ti-Nb alloys upon cooling. Acta Mater. 2024;262:119409.
50. Hildyard EM, Connor LD, Owen LR, Rugg D, Martin N, Stone HJ, et al. The influence of microstructural condition on the phase transformations in Ti-24Nb (at.%). Acta Mater. 2020;199:129-40.
51. Souza SA, Manicardi RB, Ferrandini PL, Afonso CRM, Ramirez AJ, Caram R. Effect of the addition of Ta on microstructure and properties of Ti-Nb alloys. J Alloys Compd. 2010;504(2):330-40.
52. Moffat DL, Larbalestier DC. The competition between Martensite and 0mega in quenched Ti-Nb alloys. Metall Trans, A, Phys Metall Mater Sci. 1988;19A:1677-86.
53. Cremasco A, Osório WR, Freire CMA, Garcia A, Caram R. Electrochemical corrosion behavior of a Ti-35Nb alloy for medical prostheses. Electrochim Acta. 2008;53(14):4867-74.
54. Abdel-Hady M, Fuwa H, Hinoshita K, Kimura H, Shinzato Y, Morinaga M. Phase stability change with Zr content in β-type Ti-Nb alloys. Scr Mater. 2007;57:1000-3.
55. Masumoto K, Horiuchi Y, Inamura T, Hosoda H, Wakashima K, Kim HY, et al. Effects of Si addition on superelastic properties of Ti-Nb-Al biomedical shape memory alloys. Mater Sci Eng A. 2006;438-440:835-8.
56. Xu H, Du Y, Chen H, He Y, Pan Z, Schuster JC, et al. Isothermal section at 1000 °C of the Nb-Ti-Si system. J Alloys Compd. 2005;394(1-2):235-9.
57. Ballor JA, Li T, Prima F, Boehlert CJ, Devaraj A. A review of the metastable omega phase in beta titanium alloys: the phase transformation mechanisms and its effect on mechanical properties. Int Mater Rev. 2023;68(1):26-45.
58. Ma YQ, Yang SY, Jin WJ, Wang YN, Wang CP, Liu XJ. Microstructure, mechanical and shape memory properties of Ti-55Ta-xSi biomedical alloys. Trans Nonferrous Met Soc China. 2011;21(2):287-91.
59. Zhang L, Wu J. Ti_5Si_3 and Ti_5Si_3-based alloys: alloying behavior, microstructure and mechanical property evaluation. Acta Metall. 1998;46(10):3535-46.
60. Shimagami K, Ito T, Toda Y, Yumoto A, Yamabe-Mitarai Y. Effects of Zr and Si addition on high-temperature mechanical properties and microstructure in Ti-10Al-2Nb-based alloys. Mater Sci Eng A. 2019;756:46-53.
61. Wang X, Wang L, Wang QJ, Wu YD, Si JJ, Hui XD. Enhanced mechanical properties and structure stability induced by Si in Ti–8.5Al–1.5Mo alloys. Mater Sci Eng A. 2016;676:304-11.
62. Zhang DC, Mao YF, Li YL, Li JJ, Yuan M, Lin JG. Effect of ternary alloying elements on microstructure and superelastictity of Ti–Nb alloys. Mater Sci Eng A. 2013;559:706-10.

63. Ferreira CP, Gonçalves MC, Caram R, Bertazzoli R, Rodrigues CA. Effects of substrate microstructure on the formation of oriented oxide nanotube arrays on Ti and Ti alloys. Appl Surf Sci. 2013;285P:226-34.
64. Madian M, Giebeler L, Klose M, Uhlemann M, Gebert A, Oswald S, et al. Self-organized TiO_2/CoO nanotubes as potential anode materials for lithium ion batteries. ACS Sustain Chem& Eng. 2015;3(5):909-19.
65. Ding D, Ning C, Huang L, Jin F, Hao Y, Bai S, et al. Anodic fabrication and bioactivity of Nb-doped TiO_2 nanotubes. Nanotechnology. 2009;20:305103.
66. Kulkarni M, Mazare A, Gongadze E, Perutkova Š, Kralj-Iglic V, Milošev I, et al. Titanium nanostructures for biomedical applications. Nanotechnology. 2015;26:062002.
67. Schmuki P. Self-organized oxide nanotube layers on titanium and other transition metals. In: Schmuki P, Virtanen S, editors. Electrochemistry at the nanoscale. New York: Springer; 2009. (Nanostructure Science and Technology).
68. Macak JM, Jarosova M, Jäger A, Sopha H, Klementová M. Influence of the Ti microstructure on anodic self-organized TiO_2 nanotube layers produced in ethylene glycol electrolytes. Appl Surf Sci. 2016;371:607-12.
69. Sopha H, Tesar K, Knotek P, Jäger A, Hromadko L, Macak JM. TiO_2 nanotubes grown on Ti substrates with different microstructure. Mater Res Bull. 2018;103:197-204.
70. Melo CC, Silva LS, Cremasco A, Caram R. TiO_2 nanostructured layer formation on Ti-35Nb and Ti-35Nb-5Ta samples: impact of Ta addition on polymorphic transformation and oxide composition. Mater Lett. 2024;355:135450.
71. Yasuda K, Macak JM, Berger S, Ghicov A, Schmuki P. Mechanistic aspects of the self-organization process for oxide nanotube formation on valve metals. J Electrochem Soc. 2007;154(9):C472-8.
72. Chernozem RV, Surmeneva MA, Ignatov VP, Peltek OO, Goncharenko AA, Muslimov AR, et al. Comprehensive characterization of titania nanotubes fabricated on Ti-Nb alloys: surface topography, structure, physicomechanical behavior, and a cell culture assay. ACS Biomater Sci Eng. 2020;6(3):1487-99.
73. Liu G, Du K, Wang K. Surface wettability of TiO_2 nanotube arrays prepared by electrochemical anodization. Appl Surf Sci. 2016;388:313-20.
74. Lv L, Li K, Xie Y, Cao Y, Zheng X. Enhanced osteogenic activity of anatase TiO_2 film: surface hydroxyl groups induce conformational changes in fibronectin. Mater Sci Eng C. 2017;78:96-104.
75. Shin DH, Shokuhfar T, Choi CK, Lee SH, Friedrich C. Wettability changes of TiO_2 nanotube surfaces. Nanotechnology. 2011;22:315704.
76. Kulkarni M, Patil-Sen Y, Junkar I, Kulkarni CV, Lorenzetti M, Iglič A. Wettability studies of topologically distinct Titanium surfaces. Colloids Surf B Biointerfaces. 2015;129:47-53.
77. Wang Y, Wen C, Hodgson P, Li Y. Biocompatibility of TiO_2 nanotubes with different topographies. J Biomed Mater Res A. 2013;00A:1-9.
78. Majhy B, Priyadarshini P, Sen AK. Effect of surface energy and roughness on cell adhesion and growth – facile surface modification for enhanced cell culture. RSC Adv. 2021;11:15467-76.

Data Availability

The entire dataset supporting the results of this study is available upon request from the corresponding author.